

Special Section: Noninvasive
Imaging of Processes in
Natural Porous Media



Core Ideas

- Three-dimensional X-ray imaging is a valuable tool for vadose zone research.
- Quantitative 3-D X-ray image analyses require a large amount of time and expertise.
- SoilJ is an X-ray image processing tool for the automatized analyses of X-ray images.
- SoilJ lowers the amount of time and expertise needed to evaluate 3-D X-ray images.

Dep. of Soil and Environment, Swedish Univ. of Agricultural Sciences, Box 7014, 750 07 Uppsala, Sweden. *Corresponding author (john.koestel@slu.se).

Received 18 Mar. 2017.
Accepted 22 June 2017.
Supplemental material online.

Koestel, J. 2017. SoilJ: An ImageJ plugin for the semiautomatic processing of three dimensional x-ray images of soils. *Vadose Zone J.* doi:10.2136/vzj2017.03.0062

© Soil Science Society of America.
This is an open access article distributed under the CC BY-NC-ND license (<http://creativecommons.org/licenses/by-nc-nd/4.0/>).

SoilJ: An ImageJ Plugin for the Semiautomatic Processing of Three-Dimensional X-ray Images of Soils

John Koestel*

Noninvasive three- and four-dimensional X-ray imaging approaches have proved to be valuable analysis tools for vadose zone research. One of the main bottlenecks for applying X-ray imaging to data sets with a large number of soil samples is the relatively large amount of time and expertise needed to extract quantitative data from the respective images. SoilJ is a plugin for the free and open imaging software ImageJ that aims at automating the corresponding processing steps for cylindrical soil columns. It includes modules for automatic column outline recognition, correction of image intensity bias, image segmentation, extraction of particulate organic matter and roots, soil surface topography detection, as well as morphology and percolation analyses. In this study, the functionality and precision of some key SoilJ features were demonstrated on five different image data sets of soils. SoilJ has proved to be useful for strongly decreasing the amount of time required for image processing of large image data sets. At the same time, it allows researchers with little experience in image processing to make use of X-ray imaging methods. The SoilJ source code is freely available and may be modified and extended at will by its users. It is intended to stimulate further community-driven development of this software.

Abbreviations: 3-D, three-dimensional; PVC, polyvinyl chloride.

Noninvasive three-dimensional (3-D) imaging of soil has become a valuable tool in vadose zone research in recent years because it allows nondestructive analyses of structures and processes within soils (Binley et al., 2015; Werth et al., 2010). X-ray tomography has proven to be especially superior to other imaging approaches in terms of spatial resolution and contrast with regard to mapping pore networks, root architectures, and distributions of soil constituents such as minerals, gravel, and sand grains (Cnudde and Boone, 2013; Helliwell et al., 2013). X-ray tomography has also been demonstrated to have a large potential to quantify dynamic processes within soil such as root development, soil structure evolution, water flow, and solute transport (Capowiez et al., 2014; Koestel and Larsbo, 2014; Sammartino et al., 2015; Tracy et al., 2015).

X-ray scanners for object sizes ranging between micrometer and decimeter scales are now commercially available (Wildenschild and Sheppard, 2013). As a result, the number of research institutions owning an X-ray scanner has been rapidly increasing during recent years. Free access to an X-ray scanner allows for studies that require a large number of 3-D X-ray images. There is also a wide array of free and proprietary software available that provides tools for quantitative image analyses (e.g., ImageJ and/or Fiji, Schindelin et al., 2012; QuantIm, Vogel et al., 2010; GeoDict, www.geodict.com; AVIZO, www.vsg3d.com; VGStudioMAX, www.volumegraphics.com). However, the software has not yet been adapted well to automating of image processing, which becomes necessary for analyzing a large number of 3-D images. This may be the largest obstacle that needs to be overcome before X-ray tomography can truly become a standard tool in soil and vadose zone research; the processing time needed per 3-D image has to be reduced to enable imaging studies with large numbers of replicates. The latter is necessary to obtain site-representative results in vadose zone studies because subsurface

structures, for example in soils, are known to exhibit strong heterogeneities (see, e.g., Sandin et al., 2017).

The SoilJ software aims at providing automated quantitative image analyses of 3-D X-ray tomography images of cylindrical soil and rock samples, thus enabling the rapid evaluation of large batches of X-ray images. Here we present the SoilJ software together with selected case scenarios as application examples. SoilJ is programmed in Java as a plugin for the open-source image processing and analysis software ImageJ and/or Fiji (Schindelin et al., 2012). As such, it also takes advantage of other plugins distributed with Fiji, such as BoneJ (bonej.org, Doube et al., 2010). SoilJ is intended for free-of-charge use in research and is open to community-driven development.

Materials and Methods

Software Description

SoilJ is a plugin for the open-source software ImageJ 1.x (Schneider et al., 2012) and is, therefore, written in the programming language Java. It is published under the GNU General Public License as defined by the Free Software Foundation (version 3 or later). SoilJ uses Apache Maven (Apache Software Foundation, <https://maven.apache.org/>) for compilation and for handling software dependencies (see Table 1 for an overview).

SoilJ includes a module for the automated detection of the outlines of a cylindrical sample. Once the outlines of the sample column in the image are known, they are used by SoilJ to rotate the sample into an upright position and to move it into the center of the image canvas. Unused parts of the image canvas are removed from the image. The top and bottom ends of the soil cylinder are then detected or defined, and unused image slices are removed. Next, SoilJ looks for the exact location of the inner and outer diameters of the sample vessel. The resulting information is used to calculate the bulk volume of the soil sample and may also be used to apply a beam-hardening correction routine. Note that SoilJ's beam-hardening correction routine may also be used to remove scattering artifacts from images of soil samples in steel columns, as was demonstrated by Hansson et al. (2017). Optionally, the gray

values of the column wall may be exploited for a calibration of the image grayscale in an approach similar to the one used in medical X-ray imaging that is named in honor of Sir Godfrey Newbold Hounsfield. Such a calibration is fundamentally necessary for time-lapse imaging approaches such those used by Koestel and Larsbo (2014). SoilJ offers extended image segmentation options as well as the possibility of analyzing joint histograms of several calibrated images. The plugin also has a routine to detect the topography of the top and bottom surfaces of the soil. Optionally, the surface topographies can be used for the SoilJ PoreSpaceAnalyzer as the top and bottom boundaries of the investigated region of interest. The median elevation of the upper surface may also be used as a reference depth to define a region of interest.

SoilJ makes use of several existing analysis tools for binary images, namely the 3-D Object Counter and the plugins for calculating the anisotropy, fractal dimension, thickness, and Euler number, all of which are bundled in the ImageJ 1.x plugin BoneJ (Doube et al., 2010). In addition, SoilJ includes the option to flag pore clusters that are connected to the top or bottom surfaces of the soil, or both, and to calculate the critical pore diameter, that is, the bottleneck in the connection from top to bottom. Properties that quantify the connectivity of pore networks, such as the percolating porosity and the connection probability (Renard and Allard, 2013) can also be derived from the SoilJ output file. Also included in SoilJ are modules for extracting the pore-size distribution as well as roots and particulate organic matter. The latter denotes all image-resolvable features that exhibit the density of fresh organic matter. Likewise, SoilJ contains a module to investigate the spatial stationarity of all the above-discussed morphological measures by evaluating subregions of interest within the image. The latter may be used to investigate the existence of representative elementary volumes of pore-network properties such as porosity or connectivity. Figure 1 illustrates the two modes available to define a series of regions of interest of varying size within the investigated image.

SoilJ is optimized for processing images in batch mode. Generally, SoilJ requires the location of a folder as an input and will subsequently process all images located within the specified folder. The functionality of SoilJ is further described in a technical manual,

Table 1. List of software dependencies for SoilJ version 1.0.19.

Software	Maven artifact ID	Maven group ID
ImageJ	ij	net.imagej
Fiji	fiji-lib	sc.fiji
Virtual Insect Brain protocol	VIB_	sc.fiji
Image Library 2	imglib2	net.imglib2
Apache Commons Math3	commons-math3	org.apache.commons
Apache Commons IO	org.apache.commons.io	org.apache.directory.studio
BoneJ (bonej.org)	not available	not available

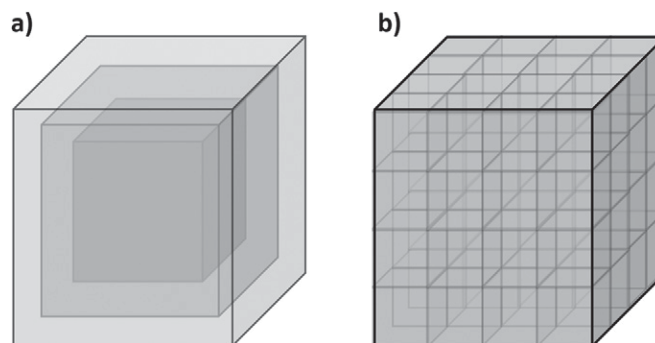


Fig. 1. Schematic illustration of the two methods of defining subregions of interest in the scale analyzer: (a) shrinkage and (b) division.

which is in the Supplemental Material. Technical details about the functioning of the different SoilJ modules can be obtained directly from the source code (version 1.0.19), which is published online together with the digital version of this manuscript.

Figure 2 illustrates the typical workflow for using SoilJ on a set of soil columns. The individual processing steps refer to modules available in SoilJ. They may be complemented by additional processing steps, as for example those proposed by Schlüter et al. (2014), using third-party software. Likewise, specific SoilJ plugins may be replaced in the image processing workflow. For example, more sophisticated approaches for image segmentation (e.g., Martín-Sotoca et al., 2017) and image bias correction (e.g., Iassonov and Tuller, 2010) may be used instead of the ones implemented in SoilJ.

Application Examples and Software Validation

Data Sets

The functionality of SoilJ is illustrated with the help of five data sets that are listed in Table 2. The respective soil samples had been collected in the framework of five different projects, referred to as SOILSPACE, Offer, Bornsjön, Allotment, and Lancaster. Some basic soil properties are shown in Table 3. More detailed information on these projects is provided in the Acknowledgments. All images were obtained with the v|tome|x 240 cone-beam X-ray scanner (General Electric) located at the Institute of Soil and Environment at the Swedish University of Agricultural Sciences.

The 89 SOILSPACE samples (aluminum, 6 cm high, 6.5-cm inner diameter) were collected manually: 43 samples from the field site in Skuterud (near Ås, Norway) and 46 from other

Table 2. An overview on the soil samples used to demonstrate the functionality of SoilJ.

Project	Sample type	Images no.	Column material	Inner diam. cm	Height cm	Resolution μm
SOILSPACE	individual samples	89	aluminum	6.5	6	40 and 80
Offer	individual samples	64	PVC	6.7	10	65
Bornsjön	individual samples	32	PVC	12.7	20	114
Allotment	time series	3	PVC	6.7	10	65
Lancaster	time series	3	Plexiglas	2.5	6	85

sampling sites across Norway. The samples were collected in 2015 and 2016 to analyze the relationships between pore-network and hydraulic properties.

The Offer samples (polyvinyl chloride [PVC], 10 cm high, 6.7-cm inner diameter) were taken from the Offer long-term crop rotation experiment in Ångermanland (Sweden) in 2013 and 2014 using a drop hammer (Jarvis et al., 2017). The Bornsjön samples (PVC, 20 cm high, 12.7-cm inner diameter) were acquired using a tractor-mounted hydraulic press from the Bornsjön soil management experimental site near Stockholm (Sweden; see, e.g., Ulén and Etana, 2014).

The Allotment sample is an example of consecutive imaging of an individual soil sample installed in a garden soil near Uppsala (Sweden). During a period of 2 yr, the soil column was repeatedly removed from the garden plot for scanning and subsequently replaced into the soil at exactly the same location. Three snapshots

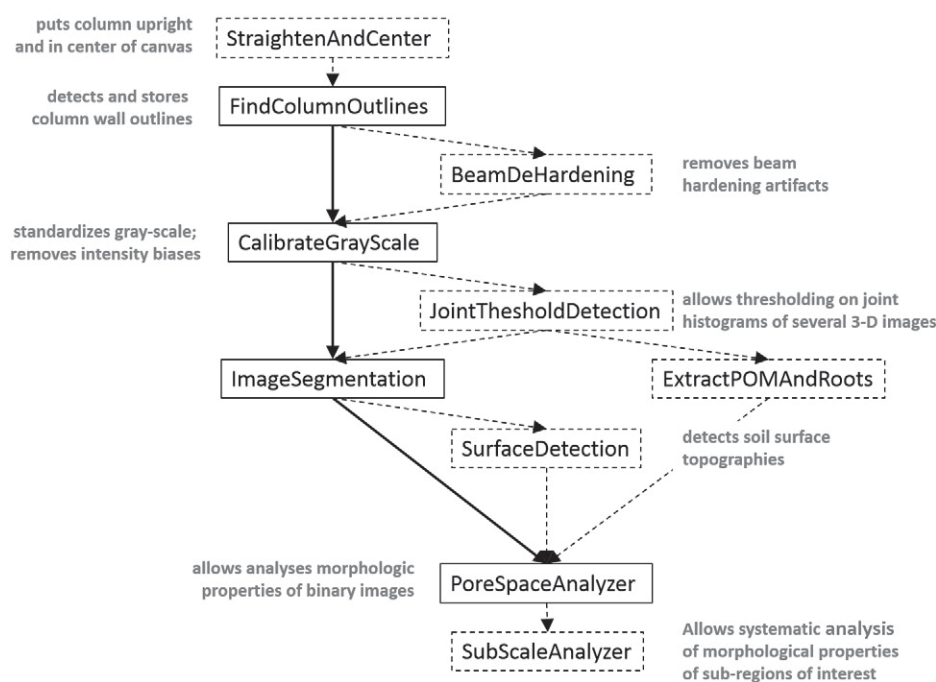


Fig. 2. The typical workflow for quantitative image processing using SoilJ is depicted with solid-line arrows and box frames. Optional SoilJ image processing steps are shown with dashed lines and arrows.

Table 3. Properties of the soils investigated in this study.

Project	Sample type	Sampling sites	Soil treatments	Soil texture	Clay content	Organic C content
		no.	no.			g g ⁻¹
SOILSPACE	undisturbed	16	–	diverse	na†	na
Offer	undisturbed	1	4	silt loam	0.23–0.4	0.013–0.041
Bornsjön	undisturbed	1	4	silty clay	0.462–0.51	0.021–0.026
Allotment	undisturbed	1	1	sandy loam	0.195	0.022
Lancaster	repacked	1	1	sandy loam	0.126	0.018

† na, not available.

from the year 2014 are shown here to illustrate the potential use of SoilJ to monitor root growth.

The Lancaster sample demonstrates the usefulness of SoilJ for time-lapse imaging. This sample consisted of repacked soil. Transport of gold nanoparticles was investigated under steady-state saturated upward flow conditions. One X-ray image was taken of the saturated column prior to the transport experiment, another one after the injection of two pore volumes of gold nanoparticles for approximately 35 min, and a final one after subsequently flushing the column with artificial rainwater for four pore volumes (approximately 70 min).

Application of SoilJ

All processing steps framed with solid lines in Fig. 2 were applied consecutively for the SOILSPACE, Offer, Bornsjön, and Allotment samples. The SOILSPACE, Offer, and Bornsjön samples were subsequently used to investigate the precision of the automatic column outline detection. The SOILSPACE columns offered the possibility of detecting both outer and inner column perimeters due to the superior density contrast between soil and aluminum compared with that between soil and PVC. The uppermost 800 image layers (approximately 55% of the column height) were used for each column to calculate the standard deviation of the detected wall thickness. A larger fraction of the column height could not be used due to a very elongated bevel at the bottom of the columns (see Fig. 3).

The SOILSPACE samples were used to illustrate how an average percolation threshold for a data set of binary 3-D images can be calculated. The image-resolvable porosity and its percolating fraction were extracted from a cylindrical region of interest (2.8-cm height, 4.9-cm diameter) from these columns (image resolution: 40 μm). By definition, the percolation threshold is the smallest porosity at which the network percolates. This threshold is exactly determined for random and effectively infinite systems but defined less well for real pore networks. In real pore networks, the percolation transition is obscured by the effects of finite sample sizes, especially in combination with correlated structures (Jarvis et al., 2017). It is therefore practical to define an average percolation threshold of an ensemble of pore networks as the porosity

for which the probability of percolation is >0.5, in other words as the smallest porosity for which the ratio between percolating and non-percolating pore networks is 1.

The performance of the SoilJ routine for calculating critical pore diameters was appraised by comparing the results for 11 SOILSPACE columns (image resolution was reduced to 80 μm; see Table 2) with those obtained with the commercial GeoDict software. The remaining SoilJ image analysis tools are either standalone ImageJ plugins or are included in the BoneJ plugin bundle. They were validated and discussed by Doube et al. (2010) as well as Schneider et al. (2012) and Schindelin et al. (2012).

The Offer samples furthermore served to demonstrate the routine for finding the soil surface topographies. The knowledge of the location of the top and bottom soil surfaces is needed to determine the soil bulk volume, which is needed to calculate the image-resolved porosity. An illustration of the beam-hardening correction approach is shown for the Bornsjön samples. The



Fig. 3. Example for the automatically detected soil column outlines (red) for one of the SOILSPACE columns (see Table 2). The figure is an example of one of the images that are created and saved by SoilJ for each processed soil column for validation purposes.

extraction algorithm for particulate organic matter and roots was tested on the time-series images of the Allotment sample. The 3-D view of the extracted organic matter and roots were created using Drishti (Limaye, 2012).

Finally, the Lancaster sample was included to illustrate SoilJ's potential to prepare X-ray images for time-lapse difference imaging. The imaging approach is similar to that described by Koestel and Larsbo (2014). SoilJ was used to calibrate the image grayscale by using the gray values of the column wall and the surrounding air as reference values. Next, all images were registered using the approach described by Preibisch et al. (2010). The difference images were then obtained by subtracting the initial reference image without the gold nanoparticles from an image of the column after the gold nanoparticles had been injected. This resulted in an image of the density increase due to the gold nanoparticles. Three-dimensional views of the location of the density changes caused by the gold nanoparticles were visualized using the Drishti software (Limaye, 2012).

Results and Discussion

Figure 3 illustrates the column outline detection for one of the SOILSPACE columns. On average, the column height detected for the SOILSPACE, Offer, and Bornsjön samples was 97 to 99% of the nominal column heights (see Tables 2 and 4). The slight underestimation was in part caused by column tops and bottoms that had been cut in a slightly slanted fashion. Furthermore, Feldkamp artifacts (see, e.g., Kudo and Saito, 1994) were often found close to the column ends, which made an exact detection of the correct column outline more difficult. The presence of the Feldkamp artifacts rendered analyses of the very top and bottom-most parts of the column (i.e., the last 1%) futile. The precision of the routine to detect the column height is therefore considered adequate. Likewise, the precision of the detection of the column outlines is also satisfactory, as the average standard deviation of the column wall thicknesses for the SOILSPACE columns was less than one voxel.

The detection of the topography of the upper soil surface is shown for two Offer columns in Fig. 4. Figure 5 illustrates the effect of the approach to correct for beam hardening. The particulate organic matter and soil roots detected by SoilJ in the Allotment sample are depicted in Fig. 6 for sampling occasions in March, May, and

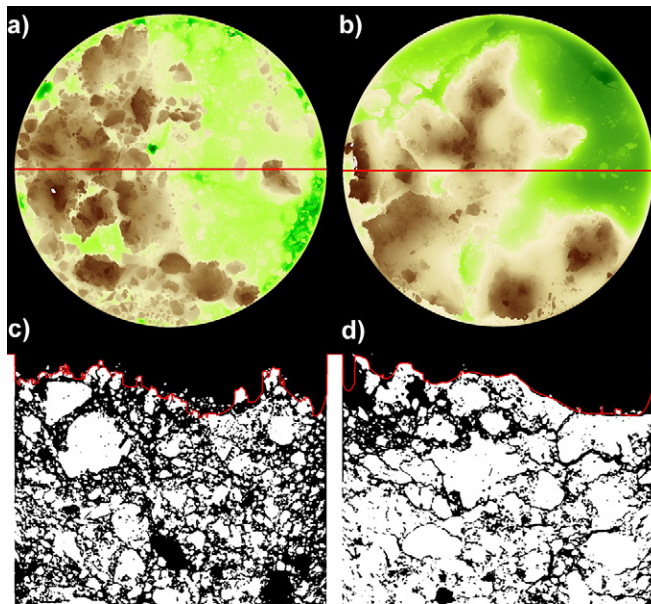


Fig. 4. The top surface topography of two Offer soil samples: (a) a soil sample with a weakly developed surface crust; (b) a soil sample with a strongly developed surface crust; (c) and (d) vertical cross-sections along the red profile lines shown in (a) and (b), respectively. Dark brown colors indicate high elevations, dark green colors low elevations, and regions that exceed the elevation of the topmost horizontal cross-section in the three-dimensional image are depicted in gray. The maximum elevation difference is 1.63 cm, and the diameter of the soil samples is 6.7 cm. The image resolution is 65 μm .

September 2014. During this period, the fraction of particulate organic matter and roots increased from 0.46 to 3.54 and 3.59% of the bulk volume thanks to the growth of a dandelion (*Taraxacum officinale* F.H. Wigg.) root. Figure 7 illustrates how the percolating properties derived in SoilJ may be used to calculate an average percolation threshold for a set of binary X-ray images or regions of interest within these images.

Uncertainty in these procedures may have introduced errors into these estimates, but they should still provide an unbiased estimate

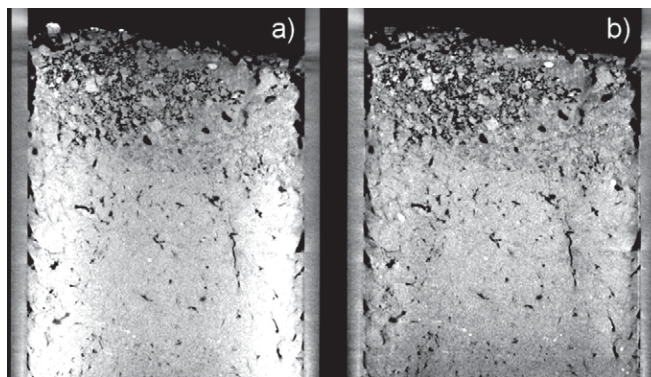


Fig. 5. A vertical cross-section of a three-dimensional X-ray image of one of the Bornsjön columns (a) before and (b) after applying the SoilJ beam-hardening correction. The image resolution is 114 μm . The gray scale is optimized to illustrate beam-hardening artifacts.

Table 4. Statistics on the precision of SoilJ's automatic column outline detection.

Project	Mean detected column height	SD of detected column height	SD deviation of detected wall thickness
	cm		voxel
SOILSPACE	5.84	0.08	0.69
Offer	9.86	0.3	not applicable
Bornsjön	19.82	0.54	not applicable

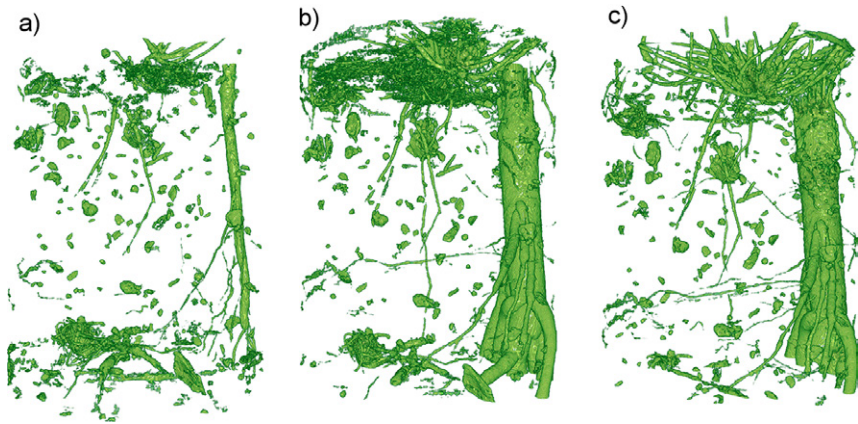


Fig. 6. A three-dimensional representation of particulate organic matter and soil roots from a soil column (10-cm height, 6.7-cm diameter, X-ray image resolution of 65 μm) on three different sampling occasions on (a) 18 May and (b) 30 Sept. 2014 and (c) 23 Mar. 2015. The soil column was reinstalled in the field (Uppsala, Sweden) directly after each imaging occasion. The taproot on the right of the soil column belongs to a dandelion. The particulate organic matter and soil roots were extracted from 16-bit grayscale images using SoilJ. The three-dimensional views were created with the visualization software Drishti (Limaye, 2012).

when applied in the same way to a data set of images. For example, the particulate organic matter and root extraction procedure results in an unbiased estimate of the temporal variation because the same approach was applied to all three images. A detailed evaluation of the validity and precision of these SoilJ features, as well as benchmarking against other image processing software, would be desirable (Baveye et al., 2010), but that was beyond the scope of this study.

The critical pore diameter derived by SoilJ was equal to or larger than the values obtained from GeoDict (Fig. 8). However, except for one sample, the overestimation was at most two voxels. The discrepancy was probably caused by the different approaches used for deriving the local pore diameters. SoilJ makes use of the algorithm included in the BoneJ (Doube et al., 2010) package. This algorithm first applies one dilation on the binary image to which it is applied and then determines the local diameters using structuring elements. Applying the dilation results in slightly larger diameters; however, they are still within the range of uncertainty inherent to the detection of features that are of a similar size as the image resolution. Note that for a binary medium, an isolated voxel may depict a spherical object with a diameter between 0.48 and 2.1 voxels if its center is located exactly in the center of an image voxel. As a consequence of the dilation, the SoilJ-derived diameters are up to two voxels larger than the ones obtained with GeoDict.

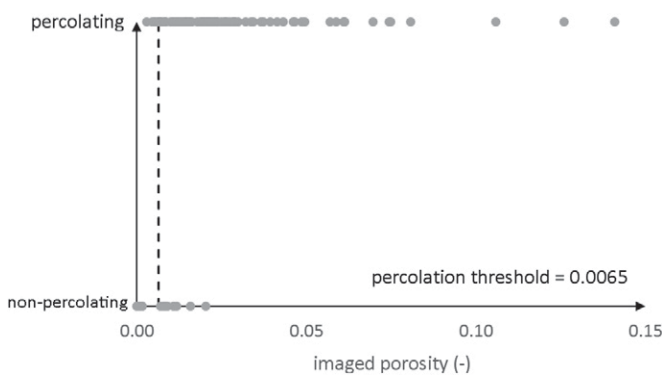


Fig. 7. The X-ray-derived porosity and the percolation threshold as defined as the smallest porosity for which the number of percolating and non-percolating pore networks are equal in number.

Occasionally, the dilation leads to the artificial fusion of neighboring pores. If such a fusion occurs at the location of the critical pore diameter, the overestimation will be even more pronounced. Visual inspection verified that this is what happened in the case of the outlier shown in Fig. 8. A refinement of the approach for mapping the local pore diameters would therefore be desirable.

Figure 9 depicts the density contrasts created by the gold nanoparticles injected into the bottom of the Lancaster column. The spiral-shaped patterns are thought to have been caused by preferential flow paths that had been created by stirring the column contents during the wet-packing procedure. SoilJ enabled efficient difference imaging due to its modules for automatic column recognition and grayscale calibration. The column recognition procedure provided a pre-alignment of the three 3-D snapshots, which is needed for the image registration. It likewise delineated the location of the column walls and surrounding air, both of which were used as reference gray values for the grayscale calibration. A quantitative evaluation of the transport experiment depicted in Fig. 9 is the subject of ongoing research.

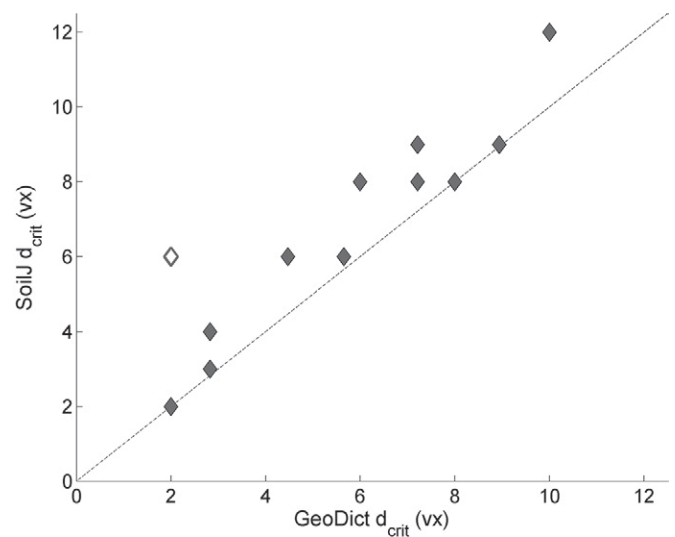


Fig. 8. Comparison of critical pore diameters (d_{crit}) derived from GeoDict and SoilJ for 11 SOILSPACE columns with percolating pore networks.

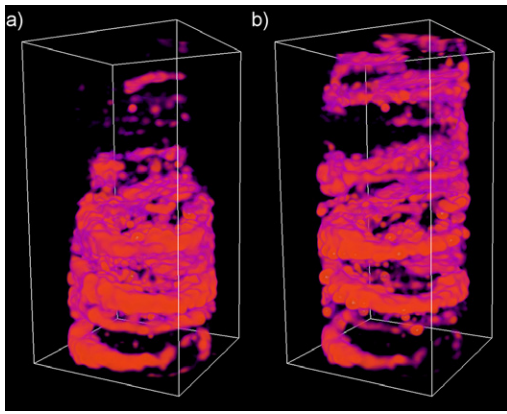


Fig. 9. Density differences caused by gold nanoparticles that were injected from the bottom: (a) after 35 min of injection and (b) after subsequent flushing of the soil column with artificial rainwater for 70 min.

Conclusion

SoilJ is a tailor-made software for the semi-automated analysis of 3-D X-ray images of soils. It facilitates the rapid extraction and quantification of structural features found within soil cores, like soil surface detection, extraction of soil particulate organic matter and roots, and quantification of pore-network connectivity. In this way, it should help to decrease the amount of time needed for 3-D image analyses, as well as lower the threshold of expertise needed to conduct quantitative X-ray image analyses of soils, thereby opening up 3-D X-ray imaging to research groups with less experience in this field. As a caveat, it should be mentioned that SoilJ has until this point only been tested on a limited number of soil column types and there is clearly no guarantee that all program modules will work error-free for all cylindrical soil columns. But like ImageJ, SoilJ is a free, open, and extensible software. We plan to promote the establishment of community-driven development of SoilJ that will extend its capabilities to additional sample geometries and include a wider array of image processing tools. This development process should be performed in close collaboration with the BoneJ and ImageJ programming initiatives.

Acknowledgments

The development of parts of this software was financed by the Research Council of Norway (NFR/FRINATEK) within the framework of Project 2013/668. Likewise, all the SOILSPACE samples were collected and analyzed for that project. The integration of the beam-hardening correction module was funded by the Swedish Research Council FORMAS Project 2013-609. The Borsnjon samples were acquired and analyzed for the same project. Collection and analyses of the Offer columns were financed by Swedish Research Council FORMAS Project 2012-572. Thanks go to Annette Dathe, Tobias Bölscher, Hannes Keck, Maryia Babko, and Muhammad Ahmad for their feedback when using the software and to Michael Doube and Richard Domander for discussions on how to implement BoneJ into SoilJ and the future of ImageJ plugins. Thanks also go to Curtis Rueden for technical advice. Finally, thanks go to the SOILSPACE consortium and the involved students and interns of NIBIO and NMBU who have sampled the respective columns; Mats Larsbo, Barbro Ulén, and Qarin Hellner, who have sampled the Borsnjon columns; Knapp Karin Norrfors and Geert Cornelis for sharing their data on the nanoparticle transport; and to Nick Jarvis for mending the English of this manuscript and discussions on percolation theory. Up-to-date versions of SoilJ as well as the SoilJ source code and the technical manual are available at <https://github.com/johnkoestel/soilj>.

References

Baveye, P.C., M. Laba, W. Offen, L. Bouckaert, P. Dello Sterpaio, R.R. Goswami, et al. 2010. Observer-dependent variability of the thresholding step in the quantitative analysis of soil images and X-ray microtomography data. *Geoderma* 157:51–63. doi:10.1016/j.geoderma.2010.03.015

- Binley, A., S.S. Hubbard, J.A. Huisman, A. Revil, D.A. Robinson, K. Singha, and L.D. Slater. 2015. The emergence of hydrogeophysics for improved understanding of subsurface processes over multiple scales. *Water Resour. Res.* 51:3837–3866. doi:10.1002/2015WR017016
- Capowiez, Y., N. Bottinelli, and P. Jouquet. 2014. Quantitative estimates of burrow construction and destruction, by anecic and endogeic earthworms in repacked soil cores. *Appl. Soil Ecol.* 74:46–50. doi:10.1016/j.apsoil.2013.09.009
- Cnudde, V., and M.N. Boone. 2013. High-resolution X-ray computed tomography in geosciences: A review of the current technology and applications. *Earth Sci. Rev.* 123:1–17. doi:10.1016/j.earscirev.2013.04.003
- Doube, M., M.M. Klosowski, I. Arganda-Carreras, F.P. Cordellieres, R.P. Dougherty, J.S. Jackson, et al. 2010. BoneJ: free and extensible bone image analysis in ImageJ. *Bone* 47:1076–1079. doi:10.1016/j.bone.2010.08.023
- Hansson, L., J. Koestel, E. Ring, and A. Gärdenas. 2017. Impacts of off-road traffic on soil physical properties of forest clear-cuts: X-ray and laboratory analysis. *Scand. J. For. Res.* (in press). doi:10.1080/02827581.2017.1339121
- Helliwell, J.R., C.J. Sturrock, K.M. Grayling, S.R. Tracy, R.J. Flavel, I.M. Young, et al. 2013. Applications of X-ray computed tomography for examining biophysical interactions and structural development in soil systems: A review. *Eur. J. Soil Sci.* 64:279–297. doi:10.1111/ejss.12028
- Iassonov, P., and M. Tuller. 2010. Application of segmentation for correction of intensity bias in X-ray computed tomography images. *Vadose Zone J.* 9:187–191. doi:10.2136/vzj2009.0042
- Jarvis, N., M. Larsbo, and J. Koestel. 2017. Connectivity and percolation of structural pore networks in a cultivated silt loam soil quantified by X-ray tomography. *Geoderma* 287:71–79. doi:10.1016/j.geoderma.2016.06.026
- Koestel, J., and M. Larsbo. 2014. Imaging and quantification of preferential solute transport in soil macropores. *Water Resour. Res.* 50:4357–4378. doi:10.1002/2014WR015351
- Kudo, H., and T. Saito. 1994. Derivation and implementation of a cone-beam reconstruction algorithm for nonplanar orbits. *IEEE Trans. Med. Imaging* 13:196–211. doi:10.1109/42.276158
- Limaye, A. 2012. Drishti: A volume exploration and presentation tool. *Proc. SPIE* 8506. doi:10.1117/12.935640
- Marín-Sotoca, J.J., A. Saa-Requejo, J.B. Grau, and A.M. Tarquis. 2017. New segmentation method based on fractal properties using singularity maps. *Geoderma* 287:40–53. doi:10.1016/j.geoderma.2016.09.005
- Preibisch, S., S. Saalfeld, J. Schindelin, and P. Tomancak. 2010. Software for bead-based registration of selective plane illumination microscopy data. *Nat. Methods* 7:418–419. doi:10.1038/nmeth0610-418
- Renard, P., and D. Allard. 2013. Connectivity metrics for subsurface flow and transport. *Adv. Water Resour.* 51:168–196. doi:10.1016/j.advwatres.2011.12.001
- Sammartino, S., A.-S. Lissy, C. Bogner, R. Van Den Bogaert, Y. Capowiez, S. Ruy, and S. Cornu. 2015. Identifying the functional macropore network related to preferential flow in structured soils. *Vadose Zone J.* 14(10). doi:10.2136/vzj2015.05.0070
- Sandin, M., J. Koestel, N. Jarvis, and M. Larsbo. 2017. Post-harvest evolution of structural pore space and saturated and near-saturated hydraulic conductivity in a clay loam soil. *Soil Tillage Res.* 165:161–168. doi:10.1016/j.still.2016.08.004
- Schindelin, J., I. Arganda-Carreras, E. Frise, V. Kaynig, M. Longair, T. Pietzsch, et al. 2012. Fiji: An open-source platform for biological-image analysis. *Nat. Methods* 9:676–682. doi:10.1038/nmeth.2019
- Schlüter, S., A. Sheppard, K. Brown, and D. Wildenschild. 2014. Image processing of multiphase images obtained via X-ray microtomography: A review. *Water Resour. Res.* 50:3615–3639. doi:10.1002/2014WR015256
- Schneider, C.A., W.S. Rasband, and K.W. Eliceiri. 2012. NIH Image to ImageJ: 25 years of image analysis. *Nat. Methods* 9:671–675. doi:10.1038/nmeth.2089
- Tracy, S.R., C.R. Black, J.A. Roberts, I.C. Dodd, and S.J. Mooney. 2015. Using X-ray computed tomography to explore the role of abscisic acid in moderating the impact of soil compaction on root system architecture. *Environ. Exp. Bot.* 110:11–18. doi:10.1016/j.envexpbot.2014.09.003
- Ulén, B. and A. Etana. 2014. Phosphorus leaching from clay soils can be counteracted by structure liming. *Acta Agric. Scand., Sect. B* 64:425–433. doi:10.1080/09064710.2014.920043
- Vogel, H.-J., U. Weller, and S. Schlüter. 2010. Quantification of soil structure based on Minkowski functions. *Comput. Geosci.* 36:1236–1245. doi:10.1016/j.cageo.2010.03.007
- Werth, C.J., C.Y. Zhang, M.L. Brusseau, M. Ostrom, and T. Baumann. 2010. A review of non-invasive imaging methods and applications in contaminant hydrogeology research. *J. Contam. Hydrol.* 113:1–24. doi:10.1016/j.jconhyd.2010.01.001
- Wildenschild, D., and A.P. Sheppard. 2013. X-ray imaging and analysis techniques for quantifying pore-scale structure and processes in subsurface porous medium systems. *Adv. Water Resour.* 51:217–246. doi:10.1016/j.advwatres.2012.07.018